Abstract #01560 ISMRM ABSTRACT

[USGOV] High-Resolution Intrinsic MRE of the Human Brain on the NexGen7T with an Anisotropic, Viscoelastic Tissue Model

Primary: Contrast Mechanisms - Elastography 〉 **Secondary:** Neuro - Neurofluids 〉 **Presentation:** Oral, PowerPitch Oral, Digital Poster, Traditional Poster 〉
Keywords: ULTRA-HIGH FIELD GLYMPHATIC SYSTEM INTRINSIC MR ELASTOGRAPHY (IMRE) HIGH SPATIAL RESOLUTION

Kulam Najmudeen Magdoom [1,2,3,4], **Oleksandr Khegai**[5,6], **Erica Walker**[5,6], **Alexander J Beckett**[5,6], **Alexandru V Avram**[4], **David Feinberg**[5,7], **An Vu**[8,9], **Peter J Basser**[4]

[1]The Henry M. Jackson Foundation for the Advancement of Military Medicine, Inc., Bethesda, United States of America
[2]Military Traumatic Brain Injury Initiative (MTBI2), Bethesda, United States of America
[3]Uniformed Services University of the Health Sciences, Bethesda, United States of America
[4]Section on Quantitative Imaging and Tissue Sciences (SQITS), Eunice Kennedy Shriver - National Institute of Child Health and Human Development (NICHD), National Institutes of Health (NIH), Bethesda, United States of America
[5]Helen Wills Neuroscience Institute, University of California Berkeley, United States of America
[6]Advanced MRI Technologies, LLC, Sebastopol, United States of America
[7]Department of Neuroscience, University of California, Berkeley, United States of America
[8]Department of Radiology and Biomedical Imaging, University Of California, San Francisco (UCSF), United States of America
[9]Northern California Institute for Research and Education, San Francisco, United States of America

Presenting Author: *Kulam Najmudeen Magdoom (magdoommohamed.kulamnajmudeen@nih.gov)*

Impact

We have developed a method to obtain high-resolution elastograms of human brain tissue without a tamper. The results indicate new contrasts compared to DTI and identifies mechanical interfaces which may be vulnerable to injuries, such as in TBI.

Synopsis

Motivation: MRE at high spatial resolution has the potential to improve tissue elasticity estimates by reducing partial volume effects.
Goals: To develop a high throughput, high resolution intrinsic MRE acquisition and analysis pipeline.
Approach: We use retrospective cardiac gated displacement imaging with very high gradient strength and slew rate at ultra-high field (UHF) to obtain displacement and diffusion tensor fields at different cardiac phases to reconstruct the viscoelasticity tensor in each voxel.
Results: The white matter was overall stiffer than gray matter. The anisotropy and magnitude of the axial and shear stiffness vary significantly within and across fiber tracts such as the corpus callosum.

Introduction

Intrinsic MR elastography (MRE) [1] based on remote palpations of the brain has the potential to detect various neurological disorders, such as traumatic brain injury (TBI), epilepsy, etc., which have so far remained invisible using traditional scans, given the high dynamic range of mechanical properties and the lack of external tamper to vibrate the tissue. Performing brain MRE at high spatial resolution increases the accuracy of stiffness estimates [2] and helps localize lesions but is challenging to acquire due to poor SNR and/or longer scan time.

We use the SNR boost from UHF along with multiband and stronger/faster gradients afforded by the NexGen7T [3] scanner to achieve 1.6x1.6x1.6 mm^3 anisotropic viscoelastic intrinsic MRE. The viscous component of the tensor indicates the fluidity of the material which can be a sensitive measure of tissue water content. We estimate the viscoelasticity tensor [4] by simultaneously measuring both the diffusion tensor (DTI) [5] and displacement vector field as a function of the cardiac phase.

Methods

MRI data was acquired in a healthy young adult on a 7T scanner (NexGen7T, Siemens Healthineers) with 200 mT/m peak gradient strength and a 900 T/m/s slew rate using an 8-channel transmit, 64-channel receive coil. Whole-brain displacement-encoded MRI data was acquired along the six directions of the icosahedron at b = 0, 700 s/mm^2 and v_{enc} = 0.6 mm/s using the CMRR Multi-band C2P (R017pre13) and the following parameters: FOV=208 x 208 x 122 mm, MB factor = 2, TR\TE = 4,500\60.4 ms, NEX = 60, and a 1.6 mm isotropic spatial resolution without GRAPPA to achieve high SNR. The total scan time is approximately 30 mins. The pulse-oximeter signal and MRI triggers were simultaneously recorded for retrospective gating.

The MRI phase unrelated to motion encoding gradients such as from RF are removed by complex division of the dataset with the b = 0 s/mm^2 scan followed by unwrapping and linear regression to remove errors arising from eddy currents, rigid body motion, etc. The displacement-encoded images were then segmented into eight different bins each roughly 120 ms in duration covering the entire cardiac cycle. Multiple repetitions of the data acquired in each bin for a given direction were utilized to reject inconsistent phase measurement in each voxel. The 3D displacement vector and the diffusion tensor fields were concurrently estimated from the phase and magnitude signals, respectively, using linear regression. The displacement vector field is Fourier transformed in time to estimate its amplitude at the cardiac frequency (i.e., ~1 Hz) which was subjected to a Helmholtz decomposition [6] with a positive definiteness constraint to estimate the voxel wise viscoelastic transverse isotropic tensor [4].

The orientation-averaged shear modulus and shear viscosity [7], and elastic and viscous components of mechanical anisotropy [4] corresponding to the real and imaginary parts of the viscoelastic tensor, respectively, are displayed as maps. The orientation dependent 4^{th}-order axial and shear stiffness tensors along with their viscous components are derived from the estimated viscoelastic tensor and projected onto a sphere which are displayed as glyphs.

Results and Discussion

The diffusion tensor and displacement vector field-derived maps from an axial slice are shown in Figure 1. The variations in DTI-derived quantities across cardiac phases were minimal given the small strains and high spatial resolution. The displacement maps show the characteristic “push-pull” and “thump” of the thalamus as shown in the left-right and feet-head components respectively [8, 9, 10]. The direction encoded color (DEC) maps at each cardiac phase were amplified 40x using the measured displacement field and shown as an animation in Figure 2. The piston like motion of the spinal cord is clearly visible with

exquisite detail. The DTI and viscoelastic parameter maps in three orthogonal planes are shown in Figure 3. While the mean diffusivity (MD) was uniform in the parenchyma, the shear modulus showed significant heterogeneity. The shear viscosity maps showed higher values in the occipital lobe. The mechanical anisotropy was accentuated compared to diffusion anisotropy with the viscous component different from the elastic component. The diffusion orientation distribution function (DT-ODF) was compared with axial and shear stiffness tensors in the corpus callosum ROI in Figure 4. While DT-ODF is uniform, the axial and shear stiffness varied significantly. The posterior portion of the corpus callosum ROI where it is straight exhibited high tensile anisotropy and low shear anisotropy compared to the anterior portion where it is curved.

Conclusion

We have demonstrated a method to obtain high-resolution *in-vivo* elastograms of the human brain without a tamper. The results showed brain deformation with fine detail and revealed new contrast not observed previously.

Acknowledgements

This study was supported by the Intramural Research Program of the Eunice Kennedy Shriver National Institute of Child Health and Human Development. This work was also supported by the Department of Defense in the Military Traumatic Brain Injury Initiative (MTBI2) under award, HU0001-22-2-0058 as well as the BRAIN Initiative (National Institutes of Health (NIH) grants: U01-EB025162, and U24-NS129949) and funding from the Weill NeuroHub. This work utilized computational resources of the NIH HPC Biowulf cluster (http://hpc.nih.gov). The views, information or content, and conclusions presented do not necessarily represent the official position or policy of, nor should any official endorsement be inferred on the part of, the Uniformed Services University, the Department of Defense, the U.S. Government or the Henry M. Jackson Foundation for the Advancement of Military Medicine, Inc.

References

1. Weaver, J. B., Pattison, A. J., McGarry, M. D., Perreard, I. M., Swienckowski, J. G., Eskey, C. J., ... & Paulsen, K. D. (2012). Brain mechanical property measurement using MRE with intrinsic activation. Physics in Medicine & Biology, 57(22), 7275.

2. Johnson, C. L., McGarry, M. D., Van Houten, E. E., Weaver, J. B., Paulsen, K. D., Sutton, B. P., & Georgiadis, J. G. (2013). Magnetic resonance elastography of the brain using multishot spiral readouts with self-navigated motion correction. Magnetic resonance in medicine, 70(2), 404-412.

3. Feinberg, David A., et al. "Next-generation MRI scanner designed for ultra-high-resolution human brain imaging at 7 Tesla." Nature methods 20.12 (2023): 2048-2057.

4. Magdoom, K. N., Avram, A. V., Sarlls, J. E., & Basser, P. J. (2025). In vivo palpation of anisotropic human brain tissue using MRI. bioRxiv, 2025-06.

5. Basser, Peter J., James Mattiello, and Denis LeBihan. "MR diffusion tensor spectroscopy and imaging." Biophysical journal 66.1 (1994): 259-267.

6. Sinkus, R., et al. "Imaging anisotropic and viscous properties of breast tissue by magnetic resonance-elastography." Magnetic Resonance in Medicine: An Official Journal of the International Society for Magnetic Resonance in Medicine 53.2 (2005): 372-387.

7. Cowin, S. C. (1989). Properties of the anisotropic elasticity tensor. The Quarterly Journal of Mechanics and Applied Mathematics, 42(2), 249-266.

8. Feinberg, D. A., & Mark, A. S. (1987). Human brain motion and cerebrospinal fluid circulation demonstrated with MR velocity imaging. Radiology, 163(3), 793-799.

9. Poncelet, B. P., Wedeen, V. J., Weisskoff, R. M., & Cohen, M. S. (1992). Brain parenchyma motion: measurement with cine echo-planar MR imaging. Radiology, 185(3), 645-651.

10. Sloots, J. J., Biessels, G. J., & Zwanenburg, J. J. (2020). Cardiac and respiration-induced brain deformations in humans quantified with high-field MRI. Neuroimage, 210, 116581.

Figures and Tables

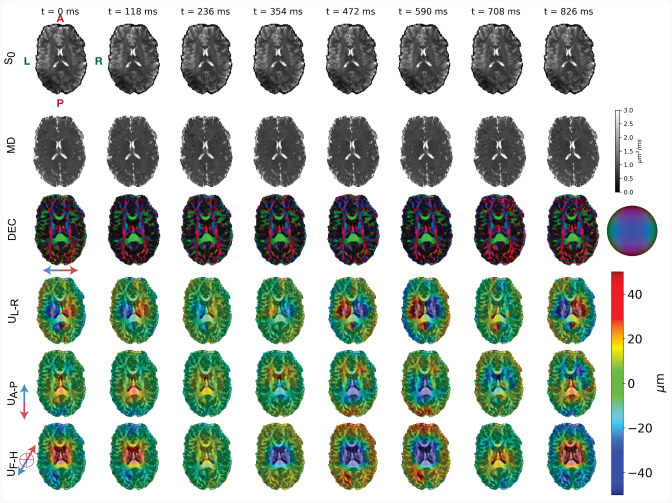

Figure 1: *Diffusion tensor and displacement vector fields at different phases of the cardiac cycle for an axial slice from a volunteer. The DTI-derived maps include S_0, mean diffusivity (MD), and direction-encoded color (DEC) along with the color sphere legend. The three components of the displacement vector field in the patient coordinate system (A - Anterior, P - Posterior, H - Head, F - Feet, R - Right, L - Left) is overlaid with a map of fractional anisotropy (FA) for anatomical context.*

Animated Figure 2

This figure contains animation/video content. To view the animation, visit the online version of this abstract.

Figure 2: *Direction encoded color (DEC) map from DTI amplified 40x using the measured 3D displacement field shown as an animation across cardiac phases to accentuate the subtle brain pulsations on all three orthogonal planes. The stretching and shearing of various white matter tracts are clearly visible.*

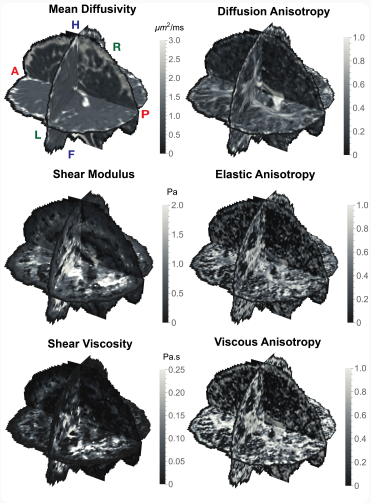

Figure 3: *Diffusion and viscoelastic tensor maps along orthogonal slices from a volunteer. These include the mean diffusivity, diffusion anisotropy (FA), elastic/viscous anisotropy, shear modulus and shear viscosity. The anatomical axes (A - Anterior, P - Posterior, H - Head, F - Foot, R - Right, L - Left) are indicated in the figure. White matter is stiffer than gray matter with differences noted among various white matter regions. The shear modulus was heterogeneous with gray-white matter contrast.*

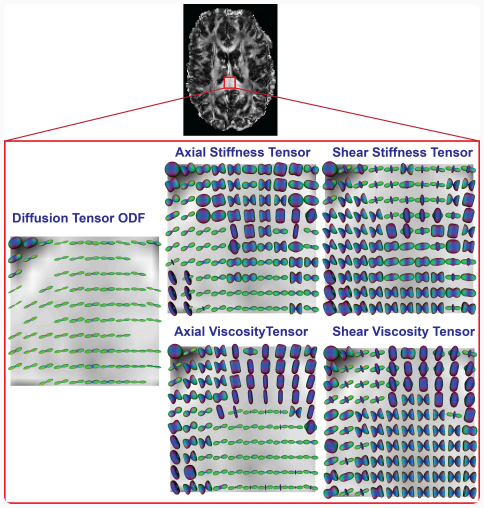

Figure 4: *Diffusion and viscoelastic tensor glyphs in corpus callosum in an axial slice from a volunteer overlaid on a fractional anisotropy (FA) map. The glyphs include the diffusion tensor orientational distribution function (DT-ODF), the axial and shear stiffness and viscosity tensors derived from the 4th order elasticity tensor. The anisotropy of the storage and loss moduli is markedly different in the ROI. Despite homogeneous DT-ODFs, mechanical property glyphs are very heterogeneous.*